RESEARCH ARTICLE OPEN ACCESS

Nonlinear Modeling of Tilting-pad Bearings with Squeeze Film Dampers and Application to Flexible Rotor Analysis

Jianming Cao[1], Timothy W. Dimond[2], Paul E. Alliare[3]
[1]*Rotor Bearing Solutions International, LLC 3277 Arbor Trace Charlottesville, VA 22911USA*
[2]*Rotor Bearing Solutions International, LLC*
[3]*Rotor Bearing Solutions International, LLC*

ABSTRACT
Linearized bearing and squeeze film damper models have limits when the rotor undergoes severe unbalance conditions or large shaft vibrations. This paper presents a nonlinear modeling approach for a complex rotor-bearing system, consisting of both tilting-pad bearings with squeeze film dampers as well as an assembly method for linear flexible rotors to simulate behavior of shaft-bearing system under severe unbalance conditions. By solving Reynolds equations derived from a tilting-pad bearing model and a finite length squeeze film damper model, the pressure profile is calculated using an approximate finite element method. The bearing/damper forces are then calculated based upon the shaft instantaneous position and velocity, and updated at each time step. The transient response of system, including coupled motions of the shaft, the bearing pads/pivots, and the dampers, is solved using a 4th Runge-Kutta integration method. The nonlinear transient behavior of a flexible eight-stage compressor under severe unbalance conditions, such as a partial impeller loss, is investigated and compared. High level shaft vibrations and nonlinear synchronous and non-synchronous behaviors at shaft and bearings are shown. The simulation shows the system damping significantly improved by installing the squeeze film dampers onto the bearings.

Date of Submission: 27 -09-2017 Date of acceptance: 10-10-2017

I. INTRODUCTION

Tilting-pad bearings with squeeze film dampers outside have been used in high-speed rotating machines to improve the system's stability through self-adopted pad angles and to decrease vibration level at the bearing location by providing additional damping. Linearized bearing model, based on the assumption of small shaft vibration (<20% of bearing clearance) around the static equilibrium position, is commonly used in rotordynamic analyses. However, the linear theory has some limits to describe, explain and predict nonlinear dynamic phenomena in rotating machines, especially for a high speed rotor under severe unbalance condition such as a blade loss in an axial compressor [1-2].Squeeze film dampers, commonly used in compressors, can only be linearized under certain conditions, such as a small whirling vibration inside the damper (a whirling orbit around the bearing centerline). For a squeeze film damper without centering spring, the whirling orbit may not be a circular orbit around the damper geometric center [3-4].

Most papers about fluid bearing or squeeze film dampers focus on solving pressure profile and characteristic linearized stiffness and damping properties at a shaft position due to static loading, using a thermo-elasto-hydrodynamic method [5-7]. For dynamic load conditions with high unbalance, however, both the location and velocity of shaft-bearing system needs to be considered as the shaft orbits in the bearing and damper clearance regions. Then nonlinear models for bearings and dampers have to be developed, especially for rotor with high level vibration. Finite element methods, based upon nonlinear analysis have been developed in rotor dynamics including a short bearing model [8], fix-pad journal bearings [9] or tilting pad bearings [10-11].The transient analysis of a squeeze film damper based on the nonlinear forces obtained from integrating the pressure profile was approached by Tao [12] and Younan [4]. The behavior of rotor dynamic systems, including both short bearing models and short bearing damper models, based on close-form equations, have been investigated by Cao [13-14]. So far few papers have been published evaluating the nonlinear behavior of rotordynamic system with the more complicated tilting pad bearing models and finite length squeeze film damper models together.

II. REYNOLDS EQUATION

The Reynolds equation represents the main governing equation to describe the behavior of the tilting-pad bearing and the squeeze film damper.

The cross section of a tilting-pad bearing geometry, in a fixed global x, y Cartesian coordinate system with its origin at the bearing center, is shown in Fig. 1 (only one pad is shown here for illustration purposes). The z axis is the axial coordinate along the bearing or damper following, the positive right-hand rule. Subject to the thin film lubrication approximation with constant pressure across the film, the governing equation of pressure profile of a tilting-pad bearing is two dimensional Reynolds equation solved on each pad. Under the assumption of an impressible laminar or turbulent Newtonian fluid with constant viscosity , the Reynolds equation in a rotating coordinate system is:

$$\frac{\partial}{\partial x}\left(\frac{h^3}{k_x\mu}\frac{\partial p}{\partial x}\right)+\frac{\partial}{\partial z}\left(\frac{h^3}{k_z\mu}\frac{\partial p}{\partial z}\right)=\frac{1}{2}\omega\frac{\partial h}{\partial \theta}+\frac{\partial h}{\partial t} \tag{1}$$

where $\partial h/\partial t$ is shaft velocity related term, and k_x, k_z are turbulence flow coefficients, which is related to local Reynolds number ($\mathrm{Re}_h = \rho R\omega h/\mu$). The following approximates are used from the Ng-Pan-Elrod Model [15]:

$$\frac{1}{k_x}=\begin{cases}\dfrac{1}{12} & \mathrm{Re}_h<100\\ \displaystyle\sum_i a_i\left(\log \mathrm{Re}_h\right)^{i-1} & 100\le \mathrm{Re}_h<10{,}000\\ 0.014-0.0114\left(\log \mathrm{Re}_h-4.0\right) & \mathrm{Re}_h\ge 10{,}000\end{cases} \tag{1a}$$

$$\frac{1}{k_z}=\begin{cases}\dfrac{1}{12} & \mathrm{Re}_h<100\\ \displaystyle\sum_i b_i\left(\log \mathrm{Re}_h\right)^{i-1} & 100\le \mathrm{Re}_h<10{,}000\\ 0.023-0.0182\left(\log \mathrm{Re}_h-4.0\right) & \mathrm{Re}_h\ge 10{,}000\end{cases} \tag{1.2}$$

$$\begin{cases}a_1=-0.4489; a_2=0.6703; a_3=-0.2904; a_4=0.0502; a_5=-0.00306\\ b_1=-0.3340; b_2=0.4772; b_3=-0.1822; b_4=0.02628; b_5=-0.001242\end{cases} \tag{1.3}$$

For laminar flow $k_x = k_z = 12$.

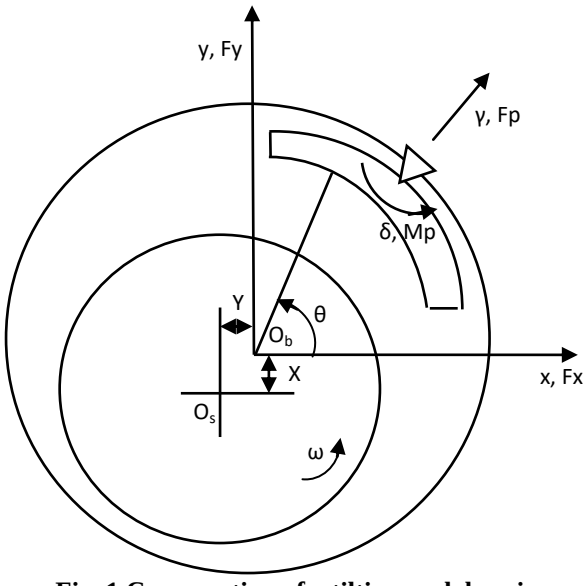

Fig. 1 Cross section of a tilting-pad bearing

These equations are applied to the tilting pad bearings and the squeeze film dampers as well. The only difference between the bearing and the squeeze film damper is the rotating speed (ω). For the bearing, the shaft inside the bearing is rotating with running speed ω and whirling inside the bearing at the same time. For the squeeze file damper, however, the bearing housing inside the squeeze film damper does not rotate, so the rotating speed (ω) for the squeeze film damper is zero. The whirl orbit and rotating speed are calculated through the time transient analysis.

The dimensionless form of Reynolds equation for each bearing pad is:

$$\frac{\partial}{\partial\theta}\left(\frac{\bar{h}^3}{k_x}\frac{\partial\bar{p}}{\partial\theta}\right)+\left(\frac{D}{L}\right)^2\frac{\partial}{\partial\bar{z}}\left(\frac{\bar{h}^3}{k_z}\frac{\partial\bar{p}}{\partial\bar{z}}\right)=\frac{1}{2}\frac{\partial\bar{h}}{\partial\theta}+\frac{\partial\bar{h}}{\partial\bar{t}} \tag{2}$$

where $\theta = x/R$, $\bar{z} = z/(L/2)$, $\bar{h} = h/C_p$, $\bar{p} = \left(C_p^2/\mu\omega R^2\right)p$ and $\bar{t} = \omega t$. The boundary conditions in circumferential direction and axial direction without axial flow in terms of the gage pressure are:

$$\begin{cases}\bar{p}(\theta_1,\bar{z})=\bar{p}(\theta_2,\bar{z})=0\\ \bar{p}(\theta,\bar{z}=\pm L/2)=0,\quad \bar{p}\ge 0\end{cases} \tag{3}$$

In this paper, the approximate finite length pressure distribution assumption in the axial direction is of the form [13]:

$$\bar{p}(\theta,\bar{z})=\bar{p}_\theta\left(1-\bar{z}^n\right) \tag{4}$$

where $\bar{p}_\theta$ is the pressure distribution at bearing center line $(\bar{z}=0)$; and *n* has different values for different L/D ratios. For example, Shelly and Ettles [16] gives *n=2* for eccentricity *ε<0.75* and *n=2.12* for *ε>0.75* when L/*D=0.5*, which indicates a short bearing.

Eq.4 is substituted into Eq.2, and integrated in the axial direction with boundary conditions given by Eq.3. The 2nd order partial differential Reynolds equation (Eq.2) is then rewritten to the following ordinary differential equation form [11,17]:

$$\frac{d}{d\theta}\left(B_1\frac{\bar{h}^3}{k_x}\frac{d\bar{p}_\theta}{d\theta}\right)+\frac{\bar{h}^3}{k_z}\left(-3\left(\frac{D}{L}\right)^2\right)\bar{p}_\theta-B_2\left(\frac{1}{2}\frac{\partial\bar{h}}{\partial\theta}+\frac{\partial\bar{h}}{\partial\bar{t}}\right)=0 \tag{5}$$

where

$$B_1=\left(\frac{n+4}{n+3}\right);\quad B_2=\left(\frac{n+1}{n}\right) \tag{6}$$

The tilting-pad bearing geometry, shown in Fig. 1, has the film thickness described as a harmonic function. The main variables in the film thickness equation are the radial clearance of the bearing (C_b), the radial clearance of each pad (C_p), the current position (*X* and *Y*) of the shaft inside the bearing, the current pad tilt angle (δ) and the current pivot position (γ). In dimensionless form, the film thickness equation is:

$$\bar{h}=1-\bar{X}\cos\theta-\bar{Y}\sin\theta-(m-\bar{\gamma})\cos(\theta-\theta_p)-\bar{\delta}\sin(\theta-\theta_p) \tag{7}$$

where $\bar{X}=X/C_p$, $\bar{Y}=Y/C_p$, $m=1-C_b/C_p$, $\bar{\gamma}=\gamma/C_p$, and $\bar{\delta}=\delta R/C_p$. The film thickness derivative with respect to time and to the angular position is:

$$\frac{d\bar{h}}{d\bar{t}}=-\dot{\bar{X}}\cos\theta-\dot{\bar{Y}}\sin\theta+\dot{\bar{\gamma}}\cos(\theta-\theta_p)-\dot{\bar{\delta}}\sin(\theta-\theta_p) \tag{8}$$

$$\frac{d\bar{h}}{d\theta}=\bar{X}\sin\theta-\bar{Y}\cos\theta+(m-\bar{\gamma})\sin(\theta-\theta_p)-\bar{\delta}\cos(\theta-\theta_p) \tag{9}$$

It is important to mention that the pressure solution form in Eq. 2 is a function of the position and velocity of the shaft center, each pad and each pivot. For given displacements and velocities of the shaft center and each pad/pivot of the bearing, based on finite element method, the pressure profile on each pad can be solved using Eq.5. The nonlinear forces and moments then can be calculated by integrating the pressure on each bearing pad in global coordinates. During the integration, only the positive pressures will be integrated, to take into account cavitation in the oil films.

$$F_{b,x}=2\int_0^{L/2}\left(\sum_{\theta_1}^{\theta_2}p(\theta,z)R\cos\theta d\theta\right)dz \tag{10}$$

$$F_{b,y}=2\int_0^{L/2}\left(\sum_{\theta_1}^{\theta_2}p(\theta,z)R\sin\theta d\theta\right)dz \tag{11}$$

$$F_p=2\int_0^{L/2}\left(\sum_{\theta_1}^{\theta_2}p(\theta,z)Rd\theta\right)dz \tag{12}$$

$$M_p=2\int_0^{L/2}\left(\left(\sum_{\theta_1}^{\theta_2}p(\theta,z)Rd\theta\right)\left(-R\sin(\theta-\theta_p)\right)\right)dz \tag{13}$$

As mentioned at the beginning of this section, the finite length damper only experiences the whirling

speed since the bearing housing does not rotate ($\omega=0$).A similar method of solving Reynolds equation is given in Appendix A.

III. EQUATION OF MOTION

To calculate the coupled motion of shaft, bearings and squeeze film dampers, a shaft finite element, with 4 degrees of freedom (DOF) per node point, is applied to model the linear shaft of the complex rotor system based on the finite element (FE) method. The cross section of a journal bearing with a squeeze film damper outside is illustrated in Fig.2.

The shaft is assumed to be axially symmetric and modeled with a Timoshenko beam element using the nodal the lateral displacements (x, y, θ_x, θ_y). The rotor built-on components, such blades, discs and impellers, are modeled as lumped parameters with mass and polar-transverse moments of inertia. An additional node, with 2 DOF (γ, δ) for the pad tilt angle and pivot displacement is added for each pad to indicate pad behavior. Also a 2-DOF node with displacements (x_{sd}, y_{sd}) is added for each squeeze film damper (SFD) to indicate the motion of bearing housing inside the squeeze film damper. Gyroscopic effects, which are a linear function of rotational speed, are taken into consideration. Bearings or squeeze film dampers are treated as nonlinear components described by the nonlinear bearing and damper forces and moments, due to the lubricant pressures, are updated at each time step based on nodal displacement and velocity.

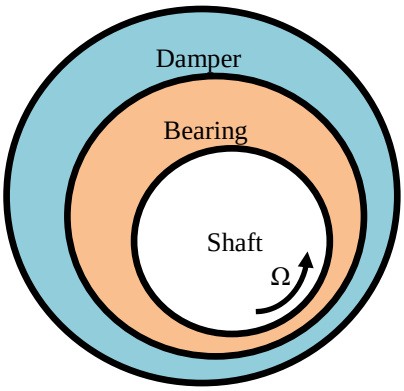

Fig. 2 Cross section of bearing with damper outside

Using the finite element method, the system equations of motion under constant operating speed are written as:

$$\begin{bmatrix} M_s & 0 & 0 \\ 0 & M_b & 0 \\ 0 & 0 & M_d \end{bmatrix} \ddot{u} + \begin{bmatrix} C_s + \Omega G & 0 & 0 \\ 0 & C_b & 0 \\ 0 & 0 & C_d \end{bmatrix} \dot{u} + \begin{bmatrix} K_s & 0 & 0 \\ 0 & K_b & 0 \\ 0 & 0 & K_d \end{bmatrix} u = F_u(t) + F_g + F_n(u, \dot{u}, t) \tag{23}$$

where M_s, C_s, G, and K_s are the mass matrix, damping matrix, gyroscope matrix and stiffness matrix from the linear rotor respectively; M_b, C_b and K_b are the pad mass, pivot damping, and pivot stiffness matrix from the tilting-pad bearing respectively; M_d, C_d and K_d are the housing mass, center spring damping and stiffness from squeeze film damper; F_u, F_g and F_n are vectors of unbalance force, gravitational force due to weight and nonlinear forces respectively. The pad mass matrix, pivot stiffness matrix and nonlinear force vector of tilting-pad bearings with total pad/pivot number of r can be written as:

$$M_b = \begin{bmatrix} I_{pad}^1 & & & \\ & M_{pad}^1 & 0 & \\ & & \ddots & \\ & 0 & & I_{pad}^r \\ & & & M_{pad}^r \end{bmatrix} \tag{24}$$

$$K_b = \begin{bmatrix} K_{pad}^1 & & & & \\ & K_{piv}^1 & & 0 & \\ & & \ddots & & \\ & 0 & & K_{pad}^r & \\ & & & & K_{piv}^r \end{bmatrix} \tag{25}$$

$$F_n = \begin{bmatrix} \cdots & F_{brg} & \cdots & M_p^k & F_p^k & \cdots & \left(F_{sfd} - F_{brg}\right) \end{bmatrix}^T \tag{26}$$

where I_{pad}^i and M_{pad}^i are inertia and mass of i^{th} pad; K_{padv}^i and K_{piv}^i are rotational and radial stiffness of i^{th} pivot; F_{brg}, M_p^i, F_p^i and F_{sfd} are bearing force, moment of i^{th} pad, force of i^{th} pivot, and damper force to bearing housing respectively. Bearing damping matrix (C_b) has similar format to Eq. 25.Rotational stiffness and damping at the bearing pivots may avoid possible numerical errors (e.g. large pad/pivot displacement) from free loaded pad/pivot effects. The displacement vector *u*, including shaft, bearing pad/pivot, and bearing housing is:

$$u = \begin{bmatrix} \cdots \underbrace{x_i \quad y_i \quad \theta_{xi} \quad \theta_{yi}}_{Shaft} \cdots \underbrace{\delta_k \quad \gamma_k}_{Pad} \cdots \underbrace{x_d \quad y_d}_{SFD} \end{bmatrix}^T \tag{27}$$

where x_i, y_i and θ_{xi}, θ_{yi} are the lateral displacements and the rotational angles of the i[th] node point along the horizontal and vertical directions respectively; δ_k and γ_k are pad tilt angle and pivot displacement of the k^{th} pad/pivot in tilting-pad bearings, and x_d, y_d are the displacements of bearing housing inside squeeze film damper.

IV. NONLINEAR TRANSIENT ANALYSIS

It is important to examine the dynamic behavior of the shaft inside the bearing for different operating rotor conditions as well as the behavior of the tilting-pad bearing and squeeze film dampers. In this work, the nonlinear analysis will enable us to examine the coupled motion of the shaft, bearing and squeeze film damper components in the time domain. The response will be studied for an example 8-stage compressor supported with two 4-pad tiling-pad bearings and two squeeze film dampers.

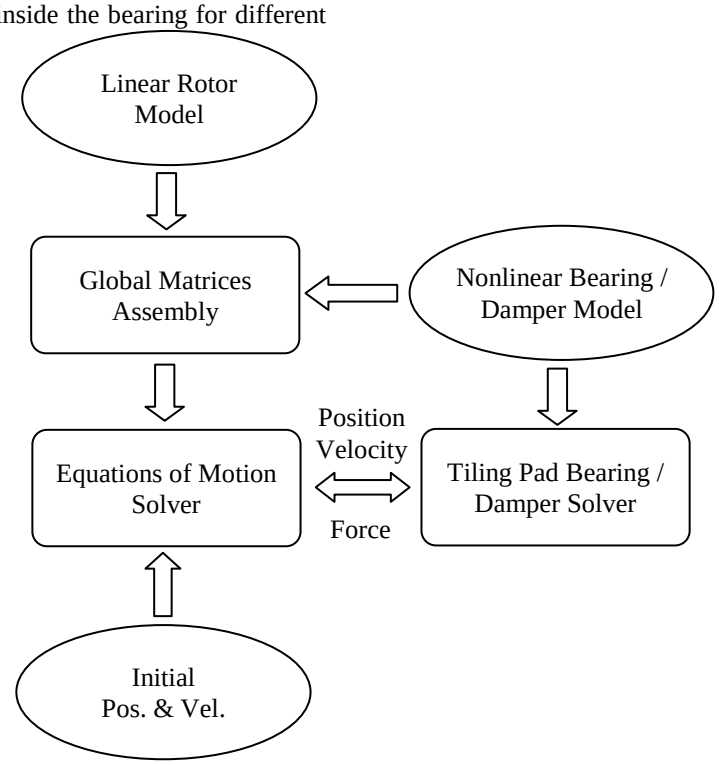

Fig. 3 Flow chart of a rotor with nonlinear bearing and damper

The nonlinear forces of the tilting-pad bearing are functions of the position and velocity of the shaft mass center, pads and pivots. The transient analysis starts from the initial position of the rotor and bearing components. The bearing forces are calculated at the initial position. From Eq. 23, the

new component positions and velocities are calculated, which are used to update the bearing forces at each time step. Figure 3 is a flowchart illustrating the calculation of the transient analysis at that time step. A 4-pad tilting-pad bearing is numerically tested for transient analysis first and used in 8-stage compressor for time transient analysis. The tilting-pad bearing information used in the model is shown in Table 1, and the geometry of the bearing including shaft, pad/pivot position and bearing clearance, is shown in Fig.4. In the figure, the clearances have been exaggerated for illustration purposes.

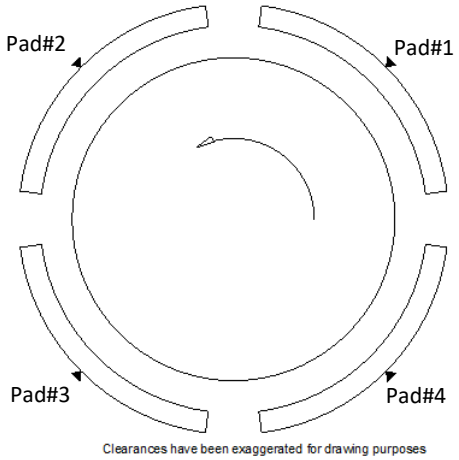

Fig. 4 Four pad tilting-pad bearing model used in analysis

The finite length squeeze film damper information is listed in Table 2. Normally the same lubricant is used for both the bearings and the dampers, but different viscosities, which are the function of the lubricant temperature, are applied here. For this bearing-damper system, the lubricant temperature inside the bearings is somewhat higher than that inside the dampers due to the higher shear effects in the bearing, length-diameter ratios, and clearances.

Table 1 Tilting-pad bearing information

Type: Tilting Pad Bearing, Load Between Pads		
Property	**Value**	**Unit**
Pad Angle	5 π /12	Rad
Pivot Location	π/4, 3 π /4, 5 π /4, 7 π /4	Rad
Offset	50%	
Length	0.1524	M
Diameter	0.1524	M
Preload	0	
Bearing Clearance	1.524×10^{-4}	M
Pad Clearance	1.524×10^{-4}	M
Oil Viscosity	1.15E-2	Pa.s
Oil Density	861	Kg/m^3
Pivot stiffness	8.756E8	N/m
Pivot damping	350	N-s/m
Pad rotational stiffness	226	N-m/rad
Pad rotational damping	0.226	N-m-s/rad

Table 2 Squeeze film damper information

Type: Finite Length Squeeze Film Damper w/o center spring		
Property	Value	Unit
Weight(Inside Damper)	27.22	kg
Length	0.1524	M
Diameter	0.254	M
Clearance	5.08×10^{-4}	M
Viscosity	0.04	Pa.s

V. PRESSURE DISTRIBUTION RESULTS

In this section, laminar flow in Eq. 5 (k_x=k_z=*12*) is used to show the effect of shaft and pad velocities. The dimensionless pressure profile of each pad is calculated with 30 circumferential elements per pad and with the assumption of n=2.25 for this bearing with L/D=1.0 for the different cases, as listed in Table 3. For Cases I&III&V, the fluid film thickness is constant ($dh/dt = 0$), those cases are same as the static analysis. The other cases (Case II&IV&VI) are all velocity related ($dh/dt \neq 0$): Case II considers the shaft center velocity ($\dot{\bar{X}}, \dot{\bar{Y}}$); Case IV involves the pivot/pad velocity in radial direction ($\dot{\bar{\gamma}}$); and Case VI includes the pad angular velocity ($\dot{\bar{\delta}}$). The pressure distributions on each pad in the circumferential direction are illustrated in Figs. 5~7. Here only the shaft and pad velocity related cases (II&IV&VI) are shown. For the zero velocity cases, the result is the same as the steady state analysis. Calculated bearing force in the x and y directions are shown in Table 3 as well. The pressure profile and the bearing forces are affected by the motion of the shaft center inside the bearing and the bearing pads/pivots.

Table 3 Tilting-pad bearing forced under different conditions

ω = 837.76 *rad/s*, $\bar{X} = 0.2, \bar{Y} = -0.1$		F_x, *N*	F_y, *N*
Case I: $\dot{\bar{X}} = \dot{\bar{Y}} = \bar{\gamma} = \bar{\delta} = \dot{\bar{\gamma}} = \dot{\bar{\delta}} = 0$		626.3	3642.2
Case II: $\dot{\bar{X}} = -0.05, \dot{\bar{Y}} = 0.05, \bar{\gamma} = \bar{\delta} = \dot{\bar{\gamma}} = \dot{\bar{\delta}} = 0$		2383.4	1621.4
Case III: $\dot{\bar{X}} = \dot{\bar{Y}} = 0, \bar{\delta} = \dot{\bar{\delta}} = 0, \dot{\bar{\gamma}} = 0$	$\bar{\gamma} = -0.05$ $\bar{\gamma} = +0.05$	450.6 769.1	3961.1 3390.0
Case IV: $\dot{\bar{X}} = \dot{\bar{Y}} = 0, \bar{\delta} = \dot{\bar{\delta}} = 0, \gamma = 0$	$\dot{\bar{\gamma}} = -0.05$ $\dot{\bar{\gamma}} = +0.05$	-1498.6 1809.1	5704.4 2264.1
Case V: $\dot{\bar{X}} = \dot{\bar{Y}} = 0, \dot{\bar{\delta}} = 0, \bar{\gamma} = \dot{\bar{\gamma}} = 0$	$\bar{\delta} = -0.1$ $\bar{\delta} = +0.1$	1796.6 -1507.1	2292.6 5571.0
Case VI: $\dot{\bar{X}} = \dot{\bar{Y}} = 0, \bar{\delta} = 0, \bar{\gamma} = \dot{\bar{\gamma}} = 0$	$\dot{\bar{\delta}} = -0.1$ $\dot{\bar{\delta}} = +0.1$	679.2 405.2	3677.8 3413.1

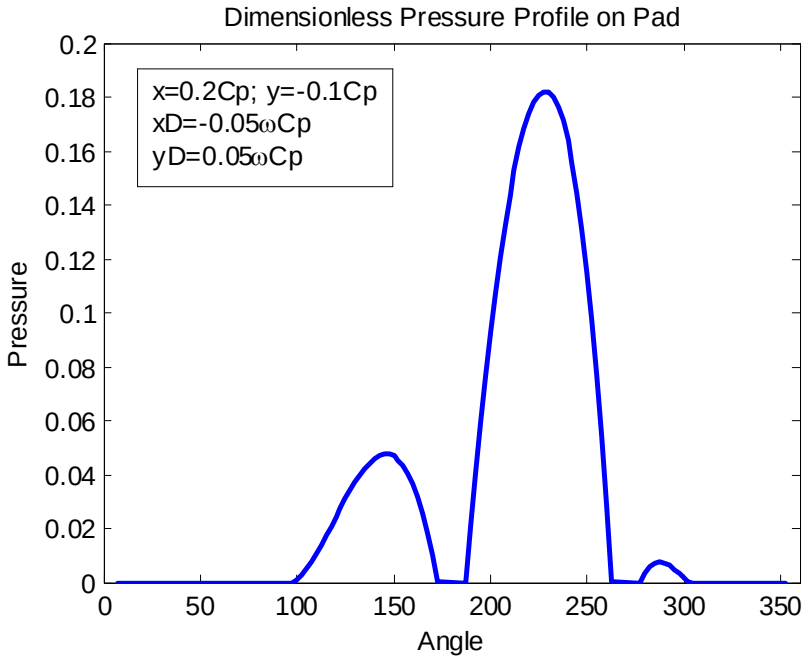

Fig. 5 Dimensionless pressure profile on pad (Case II - shaft velocity)

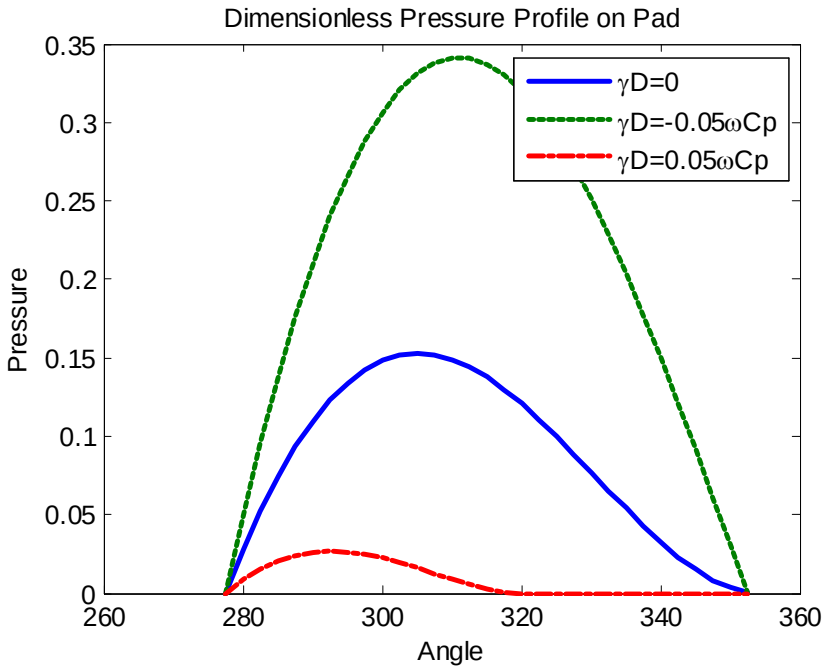

Fig. 6 Dimensionless pressure profile on pad #4 (Case IV - pivot velocity)

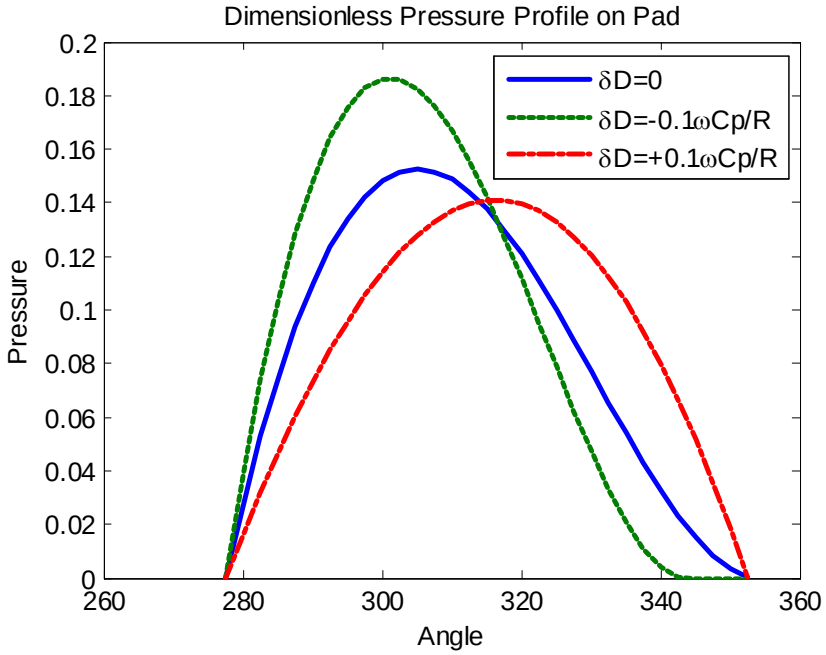

Fig. 7 Dimensionless pressure profile on pad #4 (Case VI - pad angular velocity)

The pressure profiles of the finite length squeeze film damper (given in Table 2) with different mesh densities are shown in Fig. 8. The pressure profile going through the boundary (*0* or *2π*) is continuous, and when the total number of elements increases, the curve is smoother and smoother. The finite length squeeze film damper forces vs. the total elements in circumferential direction are shown in Fig. 9. The damper force converges when the total number of elements is greater than 40. Because the nonlinear forces have to be calculated according to the instantaneous displacements and velocities at each time step, the total number of element in circumferential direction for the squeeze film damper needs to be chosen carefully to keep high accuracy, as well as to save computer run time. In this example of the 8-stage back to back industrial centrifugal compressor model, the total number of elements to calculate the finite length damper pressure profile at each time step is 60.

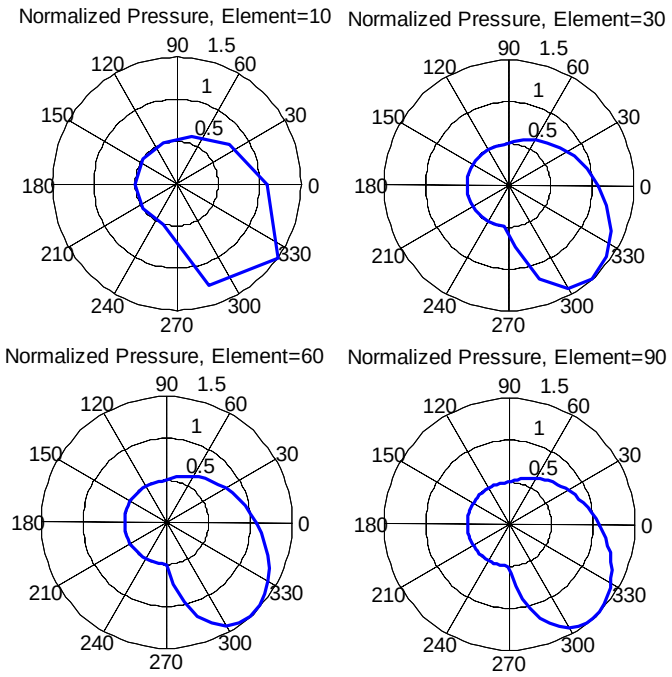

Fig.8 Pressure profiles with increasing element density

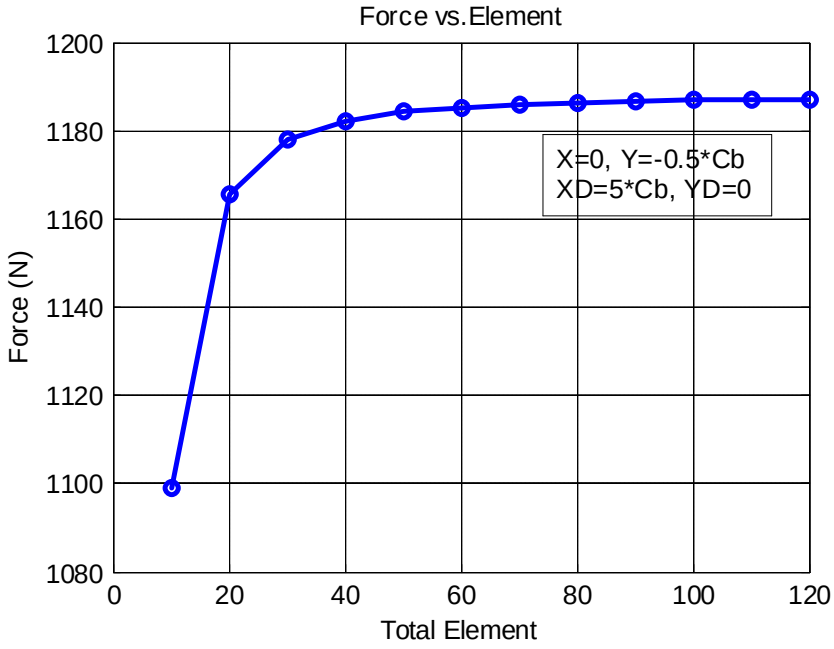

Fig.9 Damper forces vs. number ofelements

VI. TRANSIENT ANALYSIS RESULTS OF COMPLEX ROTOR

The transient analysis of aback to back 8 stage flexible centrifugal compressor rotor is evaluated in this section. The bearing dimensionless pressure profile, including the turbulence model, is shown in Eq. 5 for the pads. The turbulence coefficients k_x *and* k_z are calculated based on the local Reynolds number at each pad finite element node. The example 8-stage centrifugal compressor, which is shown in Fig. 10, is typically used for natural gas re-injection at an offshore drilling site. Table 4 lists the general compressor rotor properties of the system. The rotor has eight disks attached onto the shaft and it is supported on two tilting-pad bearings with squeeze film dampers, as shown in Fig. 2 and Tables 1&2. The rotor is modeled with 30 Timoshenko beam elements with 31 nodes. Each shaft node has four lateral degrees of freedom: two translational and two rotational. Ten additional nodes are added for 8 pads of two tilting-pad bearings and for 2 dampers. Each additional node

has two degrees of freedom. The rotor disks are modeled as lumped masses with transverse and polar moments of inertia. The whole model has 144 (31*4+8*2+2*2) degrees of freedom. The shaft and disk gyroscopic effects are calculated at the constant running speed of 837.76 *rad/s* (8,000*rpm*).The transient analysis focuses on the study of the coupled behavior of the rotor and the bearings under severe unbalance, such as due to partial impeller loss. Two different compressor running cases are simulated with properties as shown in Table 5. Based on the normal API 617 8edition requirements, twice the maximum allowable residual unbalance for this rotor should be applied for forced unbalance analysis (2*U_r, and U_r*=6350*W/N=1.025E-3 kg-m*). However, in this paper the severe unbalance conditions of 16 and 32 times the API normally required unbalance are applied, *16x (32*U_r=3.28E-2 kg-m)* and *32x (64*U_r=6.56E-2 kg-m)*are applied, as shown in Table 5.For first (16x) case, only tilting-pad bearings are considered and the second (32x) case includes both tilting-pad bearings and squeeze film dampers, due to touching of the shaft and pad.

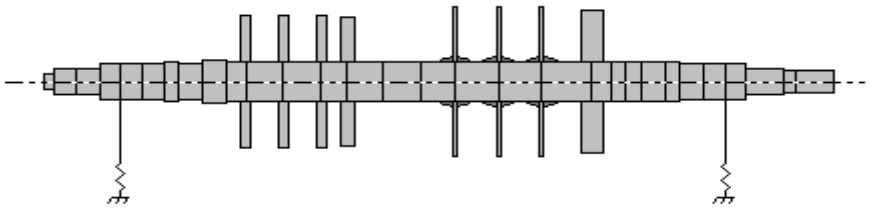

Fig. 10 Beam model of 8-stage back to back centrifugal compressor

Table 4 General information of 8-stage compressor

Property	**Value**	**Unit**
Number of disks	8	
Rotor weight	1292.28	kg
Rotor length	2.9591	M
Unbalance	2.05E-3 (API 617 8ed)	kg-m
Operating speed	837.76	rad/s
Initial time	0	S
Final time	0.1	S
Time step	8E-6	S

Table 5 Eight-stage compressor unbalance cases

Case	Location	Magnitude	Phase	Note
3	Disk #4&5	3.28E-2 kg-m	0	TPB Only
4	Disk #4&5	6.56E-2 kg-m	0	TPB+SFD

To simulate the severe condition of a sudden large unbalance force, the rotor runs 3.0 seconds under the API required unbalance (*2.05E-3 kg-m*) to obtain the steady state, then the unbalance suddenly increases at *t=3.0sec* to *3.28E-2 kg-m* (CASE 1), which is *16 times* the API required unbalance level. Due to the large sudden unbalance force, the rotor does not reach synchronous steady state response, and strong nonlinear periodic multi-circle orbits are shown. The response of the whole rotor at approximately 9.0 sec. is shown in Fig. 11.

The orbit of disk #5, and the shaft center inside left bearing, from 7.0~9.0 *sec.*, are presented in Figs. 12~14 respectively. The left bearing pad #4 displacement output plots in time and frequency domain are shown in Figs. 15~17. The rotor and bearing responses under the severe unbalance condition (Case 1) shows strongly nonlinear behavior. In Fig. 14, several peaks, including both sub&super synchronous response components, other than the synchronous peak at 837.76 *rad/s* are shown. The calculated pad force has similar frequency domain peaks as the shaft displacement have, as shown in Fig. 16.

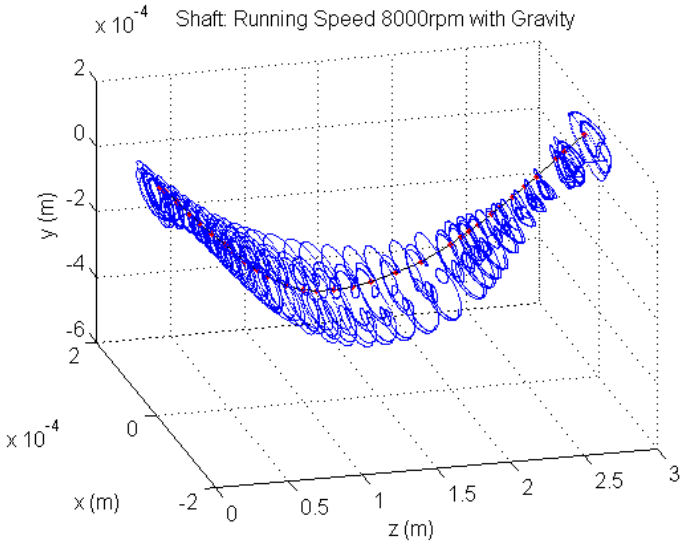

Fig. 11 Shaft orbits of CASE 1 at approximately 9.0 sec.

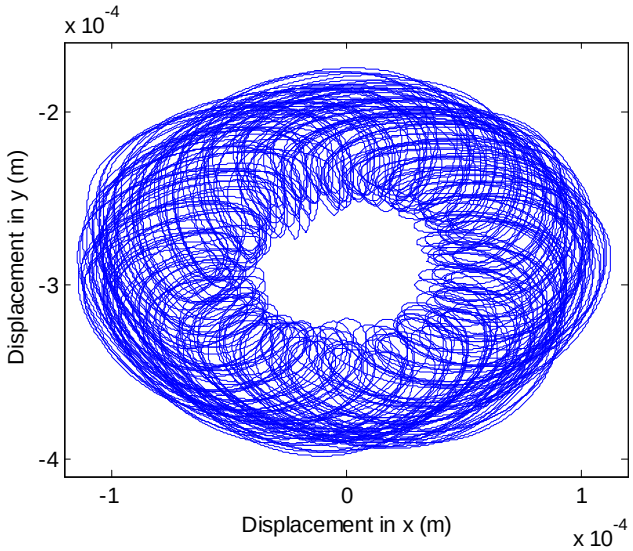

Fig. 12 Orbit of disk#5 of CASE 1, 7~9 sec.

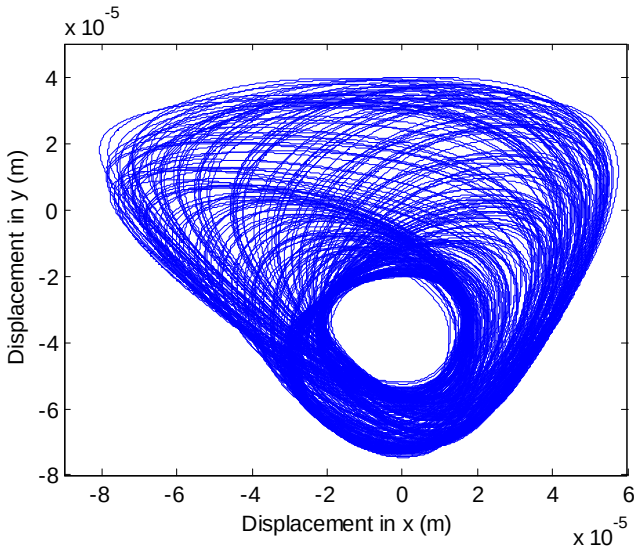

Fig. 13 Shaft center inside bearing of CASE 1, 7~9 sec.

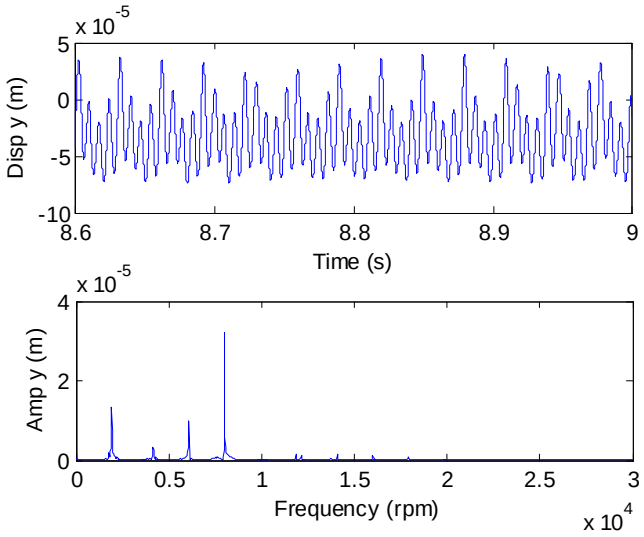

Fig. 14 FFT of shaft center inside bearing of Case 1

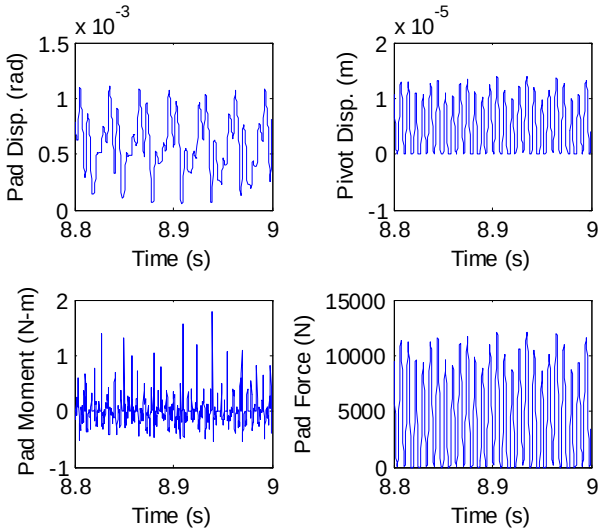

Fig. 15 Time history of bearing pad #4 of CASE 1

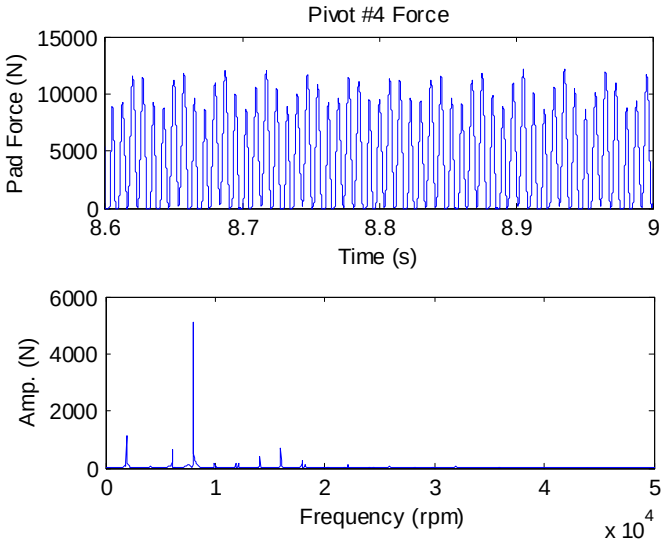

Fig. 16 FFT output of bearing pad#4 force of Case 1

When the larger unbalance is suddenly applied to the system with tilting-pad bearings only, e.g. *32 times* of API required (CASE 2, *6.56E-2kg-m*), the time transient calculation was stopped due to touching between the shaft and the bearing pads. To obtain the system response under the larger unbalance forces, the squeeze film dampers are introduced into the system to increase damping. The shaft behavior for CASE 2 is shown in Fig. 17. Now, there is no touching among the shaft, the bearing pads and the squeeze film dampers during the transient analysis. The system reaches its steady state after approximately 0.15 seconds, which is 50 times faster than the rotor without the squeeze film dampers. For the rotor on the tilting-pad bearings only, it takes at least 7.0 sec. to reach steady state under CASE 1 with the same initial conditions.

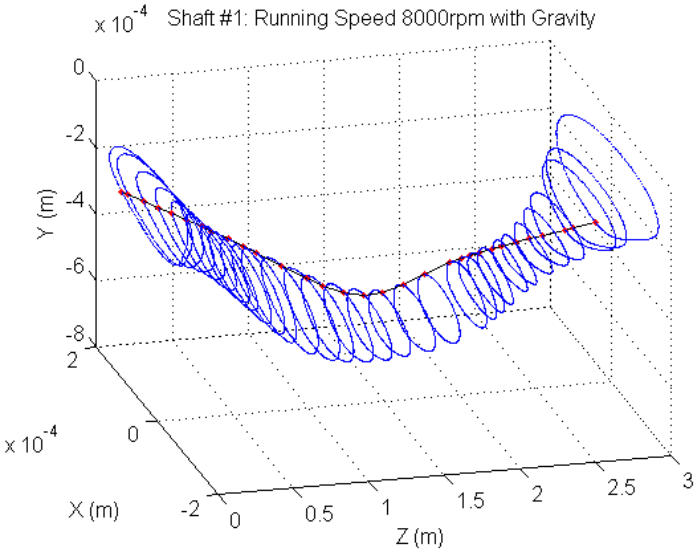

Fig.17 Shaft Orbit with SFDs at 0.5 sec, CASE 2

The response of the shaft center inside the bearings (nodes #5&#27) is presented in Fig. 18. In those figures, the red circle indicates the bearing clearance (C_b*=0.1526mm*). The response of the bearing housings, which are inside the two squeeze film dampers, is shown in Fig. 19, in which the red circle indicates the damper clearance (C_d*=0.508mm*) and the two lower plots are the detailed orbits. The steady state orbits of the bearing housings are downward (negative) in the vertical direction due to the weight of the bearing housing. Since the bearing housing orbit is not close the bottom of the damper, only synchronous response is seen from all shaft nodes, as shown in Fig 17.

The results of the nonlinear forces at node #27 from the tilting-pad bearing and the finite length squeeze film damper in time and frequency domains are shown in Figs. 20&21. Although the response of the whole shaft indicates a synchronous behavior, as shown in Fig. 17, the super-synchronous response is presented in the transient output of these nonlinear forces as shown in the frequency domain response such as shown in Figs 20&21. However, since the bearing housing orbits inside the two finite length squeeze film dampers are not close the bottom of the damper, only weakly nonlinear response is shown from those forces.

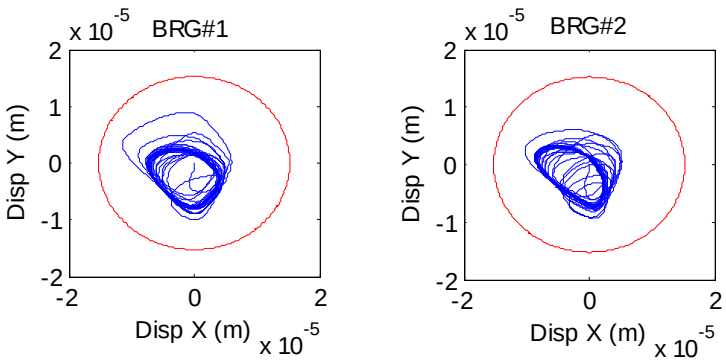

Fig.18 Bearing response at node 5&27 under CASE 2

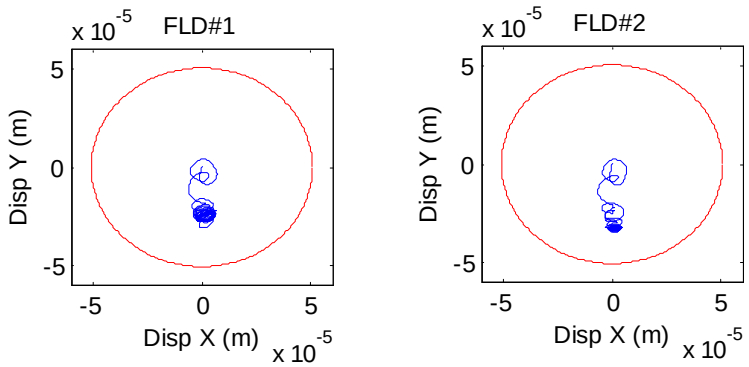

Fig. 19 SFD response at node 5&27 under CASE 2

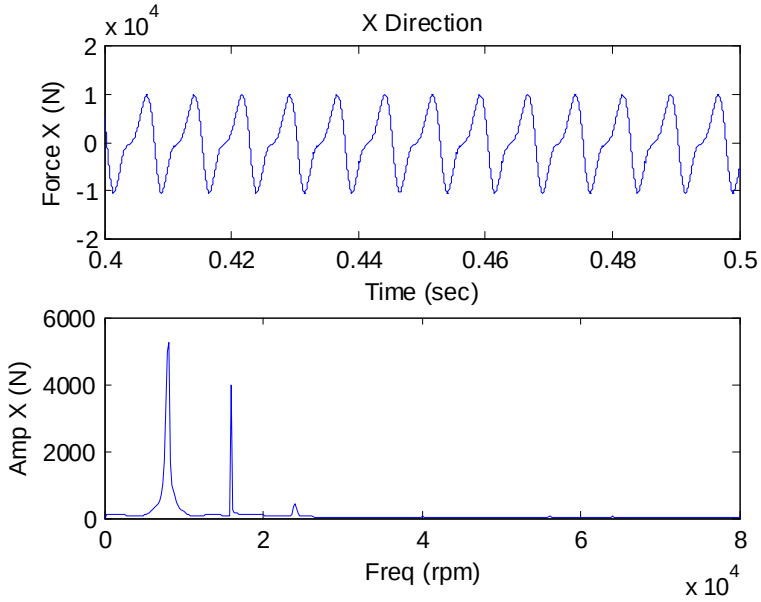

Fig.20 FFT of bearing force at node 27 under CASE 2

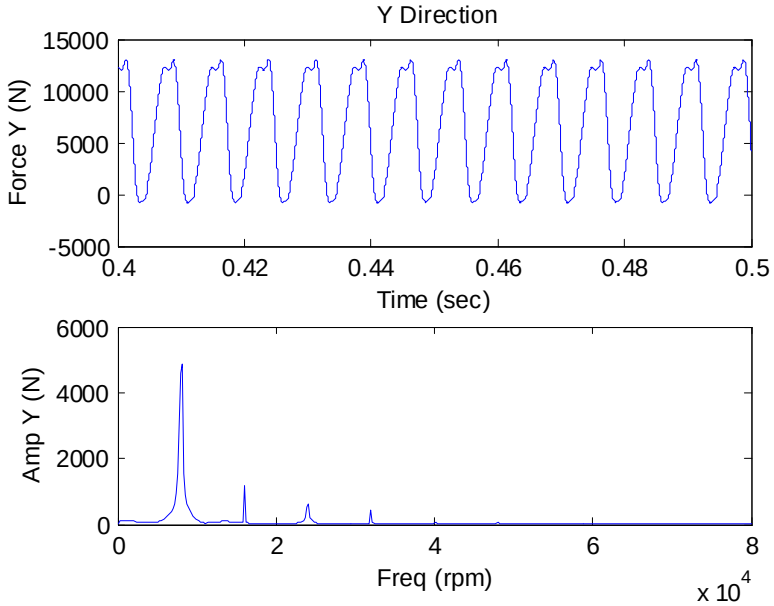

Fig. 21 FFT of SFD force at node 27 under CASE 2

No negative pressure occurs in the bearing film, the pivot force, which is calculated from the pressure profile, is always positive or zero (unloaded), as shown in Fig. 22. For the same reason, there is almost no negative pivot displacement, as shown in Fig. 23. The super-harmonic response is obtained in the pad force plots, displacement plots as well as tilt angle plots due to the periodic unloading on pad as shown in Figs. 22~24.

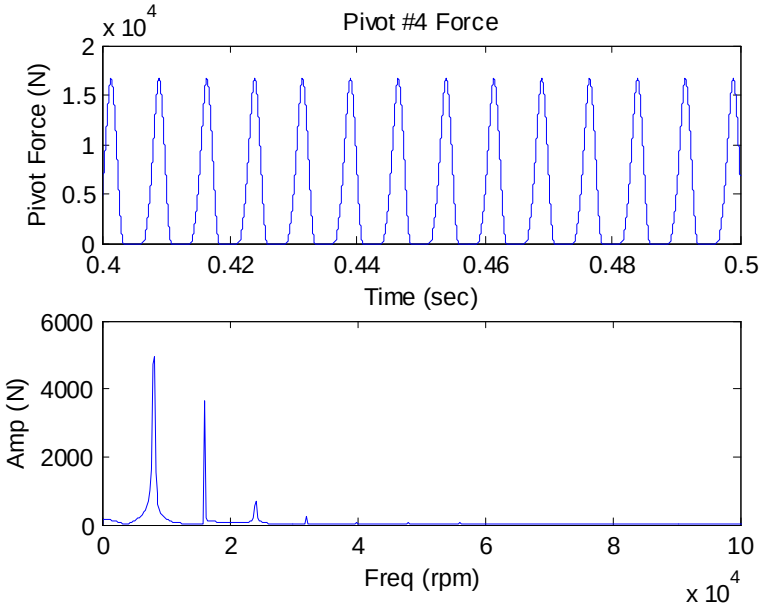

Fig. 22 FFT of bearing pad #4 force at node 27 of CASE 2

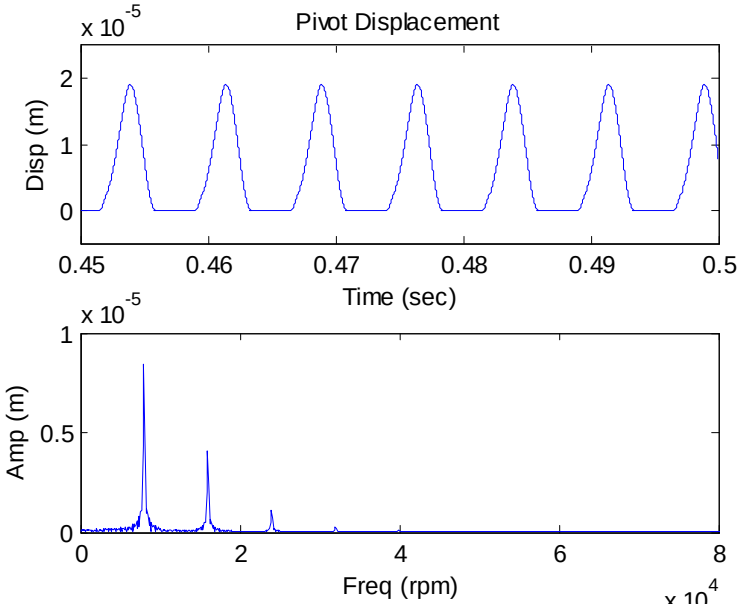

Fig.23 FFT of bearing pivot #4 displacement at node 27 of CASE 2

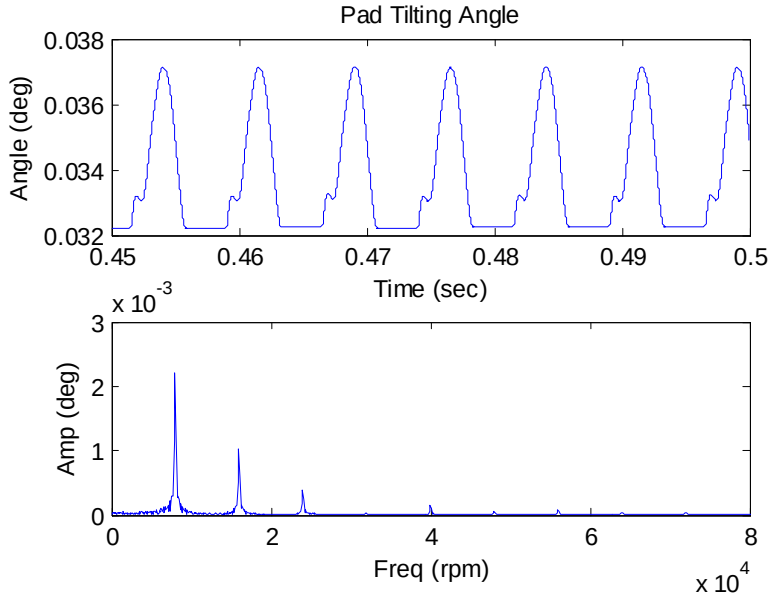

Fig. 24 FFT of bearing pad #4 tilting angle at node 27 of CASE 2

VII. CONCLUSIONS

In rotating machinery, situations occur which are not properly modeled using linearized analysis. Often, a nonlinear transient analysis is required to evaluate displacements and forces on the system components, including synchronous and non-synchronous frequency effects. This paper presents a complex nonlinear model of a shaft/tilting-pad bearing/squeeze film damper system taking into consideration the effects of the bearing pad and pivot displacements and velocities, and a nonlinear finite length squeeze film damper model. The pad/pivot effect is introduced by calculating lubricant film thickness and solving the pressure profile on each pad. The shaft position and velocity of the bearing pads and pivots affects the pressure profile significantly. An assembly method of a complex rotor supported with tilting-pad bearings and squeeze film dampers involving a large number of degrees of freedom is given. The transient analysis of an 8-stage flexible rotor supported on two tilting-pad bearings with squeeze film dampers under different severe unbalance conditions is conducted. Strong nonlinear behavior, such as sub&super synchronous response, is shown when large unbalance forces such as partial impeller loss are suddenly applied. Adding squeeze film dampers avoids possible pad/shaft touching under the severe conditions, decreases the vibration amplitude and increases the effective damping of the system.

APPENDIX A

The damper's dimensionless form of Reynolds equation with assumption laminar flow is:

$$\frac{\partial}{\partial\theta}\left(\frac{\bar{h}^3}{12}\frac{\partial\bar{p}}{\partial\theta}\right)+\left(\frac{D}{L}\right)^2\frac{\partial}{\partial\bar{z}}\left(\frac{\bar{h}^3}{12}\frac{\partial\bar{p}}{\partial\bar{z}}\right)=\frac{\partial\bar{h}}{\partial t} \tag{A1}$$

where $\theta = x/R$, $\bar{z} = z/(L/2)$, $\bar{h} = h/C_d$, and $\bar{p} = \left(C_p^2/\mu R^2\right)p$. The damper boundary conditions in the circumferential direction and axial direction, neglecting the oil supply groove in squeeze film damper, are:

$$\begin{cases}\bar{p}(0,\bar{z})=\bar{p}(2\pi,\bar{z})=0\\ \left.\dfrac{\partial\bar{p}}{\partial\theta}\right|_{\theta=0}=\left.\dfrac{\partial\bar{p}}{\partial\theta}\right|_{\theta=2\pi}\end{cases} \tag{A2}$$

$$\bar{p}(\theta,\bar{z}=\pm L/2)=0,\quad \bar{p}\ge 0 \tag{A3}$$

Using the same assumption of the pressure distribution along the axial direction (Eq. 4), the dimensionless equation to solve the pressure profile at $\bar{z}=0$ is:

$$\frac{d}{d\theta}\left(B_1\frac{\bar{h}^3}{12}\frac{d\bar{p}_\theta}{d\theta}\right)+\frac{\bar{h}^3}{12}\left(-3\left(\frac{D}{L}\right)^2\right)\bar{p}_\theta-B_2\left(\frac{\partial\bar{h}}{\partial\bar{t}}\right)=0 \tag{A4}$$

In dimensionless form, the film thickness equation is:

$$\bar{h}=1-\bar{X}\cos\theta-\bar{Y}\sin\theta \tag{A5}$$

$$\frac{d\bar{h}}{dt} = \dot{\bar{X}}\cos\theta - \dot{\bar{Y}}\sin\theta \tag{A6}$$

$$\frac{d\bar{h}}{d\theta} = \bar{X}\sin\theta - \bar{Y}\cos\theta \tag{A7}$$

For specified nodal displacements and velocities of the bearing housing inside the damper, the pressure profile of the damper can be solved and the nonlinear forces are calculated by integrating the pressure profile. Nonlinear forces in horizontal and vertical directions are evaluated as:

$$F_{d,x} = 2\int_0^{L/2}\left(\sum_0^{2\pi} p(\theta,z)R\cos\theta d\theta\right)dz \tag{A8}$$

$$F_{d,y} = 2\int_0^{L/2}\left(\sum_0^{2\pi} p(\theta,z)R\sin\theta d\theta\right)dz \tag{A9}$$

NOMENCLATURE

B_1, B_2	weight factor of axial pressure
C_b, C_d	bearing, SFD radial clearance, m
C_s	shaft damping matrix
C_p	pad radial clearance, m
D	journal diameter, m
F_{sfd}, F_{brg}	bearing, SFD forces, N
F_g	gravitational force vector
F_n	nonlinear bearing force vector
F_p	bearing pad force, n
F_u	unbalanced force vector
F_{bx}, F_{by}	bearing force in x, y direction, N
F_{dx}, F_{dy}	SFD force in x, y direction, N
G	gyroscopic matrix
h	fluid film thickness, m
$\bar{h}$	dimensionless fluid film thickness (h/C_p)
I_{pad}	pad mass moment of inertia, kg-m^2
K_{piv}	pivot stiffness. n/m
K_s	shaft stiffness matrix
k_x, k_z	Turbulence flow coefficients
L	bearing axial length, m
m	preload of tilting-pad bearing ($1-C_b/C_p$)
M_b, M_d	bearing, SFD mass matrix
M_s	shaft mass matrix
M_p	pivot moment, N-m
M_{pad}	pad mass, kg
n	axial pressure distribution factor
p	pressure in lubricant film, pa
$\bar{p}$	dimensionless pressure ($pC_p^2/\mu\omega R^2$)
R	bearing radius, m
Re_h	Local Reynolds number ($\rho R\omega h/\mu$)
t	time, sec
$\bar{t}$	dimensionless time (ωt)
$u, \dot{u}, \ddot{u}$	displacement, velocity and acceleration vectors
x_i, y_i	shaft nodal displacement, m
X, Y	displacement of shaft center in bearing, m
$\bar{X}, \bar{Y}$	dimensionless displacement of shaft center ($X/C_p, Y/C_p$)
$\dot{\bar{X}}, \dot{\bar{Y}}$	dimensionless velocity of shaft center ($\dot{X}/\omega C_p, \dot{Y}/\omega C_p$)
$\bar{z}$	dimensionless axial direction ($z/(L/2)$)
γ	bearing pivot displacement, m
$\bar{\gamma}$	dimensionless pivot displacement (γ/C_p)
$\dot{\bar{\gamma}}$	dimensionless pivot velocity ($\dot{\gamma}/\omega C_p$)
δ	bearing pad displacement (rad)
$\bar{\delta}$	dimensionless pad displacement ($\delta R/C_p$)
$\dot{\bar{\delta}}$	dimensionless pad velocity ($\dot{\delta}\omega R/C_p$)
ε	bearing eccentricity
θ_{xi}, θ_{yi}	shaft nodal rotational displacement, rad
θ_p	pivot location, rad
θ_1, θ_2	pad leading&trailing angle (rad)
μ	lubricant dynamic viscosity, pa-s
ω	shaft rotational speed inside bearing, rad/s

REFERENCES

[1] Ehrich, F. F, 2008, "Observations of Nonlinear Phenomena in Rotordynamics," JSME J. System Design and Dynamics, **2**(3), pp. 641-651

[2] Ertas, B., Cerny, V., Kim, J., and Polreich, V., 2015, " Stabilizing a 46 MW Multistage Utility Steam Turbine Using Integral Squeeze Film Bearing Support Dampers", J. Eng. Gas Turbines Power 137(5), 052506

[3] Dimond, T., Younan, A., Allaire P., and Nicholas J, 2013, "Modal Frequency Response of a Four-Pad Tilting Pad Bearing With Spherical Pivots, Finite Pivot Stiffness, and Different Pad Preloads", J. Vib. Acoust 135(4), 041101

[4] Younan, A., Cao, J., Dimond, T., and Allaire, P. E., 2011, "Nonlinear Analysis of Squeeze Film Damper with Entrained Air in Rotordynamic Systems," STLE Tribol., 54, pp. 132-144

[5] Guo, Z, Hirano, T, and Kirk, R., 2005, "Application of CFD Analysis for Rotating Machinery—Part I: Hydrodynamic, Hydrostatic Bearings and Squeeze Film Damper", J. Eng. Gas Turbines Power, 127(2), pp445-451

[6] He, M., Allaire, P. E., 2002, "Thermoelastohydrodynamic Analysis of Journal Bearings with 2D Generalized Energy Equation," IFTOMM, Sixth International Conference on Rotor Dynamics, Sydney, Australia

[7] Saeid, D., Cao, J., Younan, A., Allaire, P. and Dimond, T., 2012, "Temporal and Convective Inertia Effects in Plain Journal Bearings With Eccentricity, Velocity and Acceleration", ASME J. Tribol., 134(3), 031704

[8] Hassenpflug, H. L., 1988, "Transient Analysis of Coupled Rotor-Structure Systems," PhD Thesis, University of Virginia

[9] Zheng, T., and Hasebe, N., 2000, "Nonlinear Dynamic Behaviors of a Complex Rotor-Bearing System," J. Appl. Mech., 67, pp. 485-495.

[10] Chaa, M., Isakssonb, P. and Glavatskiha, S., 2013, "Influence of pad compliance on nonlinear dynamic characteristics of tilting pad journal bearings", Tribol Int, 57, pp 46–53

[11] Cao, J., Dimond, T., Younan, A., and Allaire P., 2013, "Nonlinear Modeling of Tilting-Pad Bearing with Application to a Flexible Rotor Analysis", ASME IDETC, Portland, OR, DETC2013-13712.

[12] Tao, L., Diaz, S., and San Andres, L. A., 2000, "Analysis of Squeeze Film Dampers with Bubbly Lubricants," ASME J. Tribol., 122, pp 205-210.

[13] Cao, J., Dimond, T. W., and Allaire P. E., 2014, "Numerical Analysis of Flexible Rotor with Nonlinear Bearings and Squeeze Film Dampers", ASME IMECE, Montreal, Canada, IMECE2014-37365

[14] Cao, J., Dimond, T. W., and Allaire P. E., 2015, "Coupled Lateral and Torsional Nonlinear Transient Rotor-Bearing System Analysis with Applications", ASME J. Dyn. Sys., Meas., Control. vol. 137(9): 091011

[15] Szeri, A. Z., 2005, "Fluid Film Lubrication: Theory and Design", Cambridge University Press

[16] P. Shellya and C. Ettles, 1970, "A Tractable Solution for Medium-Length Journal Bearings," Wear, vol. 12, pp. 221-228.

[17] Singhal, S., and Khonsari, M., 2005, "A simplified thermo-hydrodynamic stability analysis of journal bearings," Proc. Instn. Mech. Engrs., Part J: J. Engineering Tribology , 219, pp. 225-234.

Jianming Cao. "Nonlinear Modeling of Tilting-Pad Bearings with Squeeze Film Dampers and Application to Flexible Rotor Analysis." International Journal of Engineering Research and Applications (IJERA) , vol. 7, no. 10, 2017, pp. 51–68.